Chapter 2
Basics of Thermomechanics and Inelasticity

Rock salt can undergo large inelastic deformations over extended periods of time. Many analyses, however, refer to time intervals and mechanical loads that cause deformations for which the small-strain assumption remains valid. Here, we restrict ourselves to such small-strain settings and postpone analyses under finite deformations to a follow-up contribution (compare also Fig. 2.1).

OGS mainly offers the analysis types 3D, 2D plane strain and axisymmetric. In the sequel, a general tensorial notation is chosen for the field equations while finite element concepts are presented in a three-dimensional setting only. For special considerations in the context of lower-dimensional or analyses relying on special symmetries, we refer the reader to standard textbooks (Bathe 2014; Zienkiewicz et al. 2005–2006), the benchmark book series (Kolditz et al. 2012, 2014, 2016) or the source code documentation of OGS.[1]

OGS offers the possibility to couple mechanical analyses to thermal, hydraulic and chemical processes using either sequential or monolithic schemes. Here, the focus is on thermo-mechanical couplings.

2.1 Governing Equations

In a finite-strain setting, the material is mapped to different geometrical configurations as it deforms and evolves over time. The two most relevant configurations are the current and the reference configuration, cf. Fig. 2.1. The different configurations lead to a multitude of stress and strain measures. In a small-strain setting, we assume that the reference configuration (often taken as the undeformed state for convenience) changes only very slightly. Thus, particles are assigned only their reference coordinates, now designated by $\mathbf{x}$, and field gradients are evaluated

[1] https://doxygen.opengeosys.org/.

T. Nagel et al., *Computational Geotechnics*, SpringerBriefs in Energy,
DOI 10.1007/978-3-319-56962-8_2

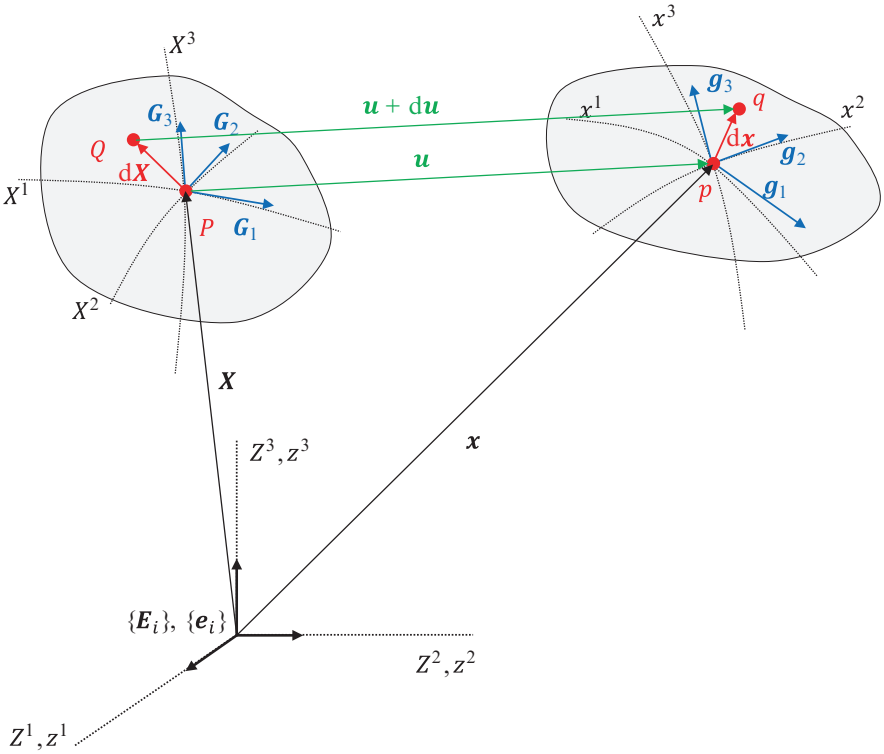

Fig. 2.1 Material points move from their reference placement **X** to their current placement **x**, both of which are connected by the displacement vector **u**. Neighbouring material points define material line elements represented by d**X** and d**x** in the reference and current configurations, respectively. Curvilinear (X^I, x^i) and Cartesian (Z^I, z^i) coordinate lines define local basis systems for the geometrical description of the motion problem. For further details, see Holzapfel (2000), Haupt (2002), and Hutter and Jöhnk (2004)

exclusively with respect to those coordinates. The relevant strain measure is the small-strain tensor $\boldsymbol{\epsilon} = \text{sym grad}\,\mathbf{u}$, the relevant stress measure the Cauchy stress tensor $\boldsymbol{\sigma}$. The initial boundary value problem is thus defined on a (reference) domain Ω as indicated in Fig. 2.2.

To perform a basic thermo-mechanical analysis in a quasistatic small-strain setting we employ the local (PDE) forms of the equilibrium conditions (derived from the balance of momentum) and the heat conduction equation (derived from the balance of energy)

$$\mathbf{0} = \text{div}\,\boldsymbol{\sigma} + \varrho\mathbf{b} \tag{2.1}$$

$$0 = \varrho c_p \frac{\partial T}{\partial t} + \text{div}\,\mathbf{q} \tag{2.2}$$

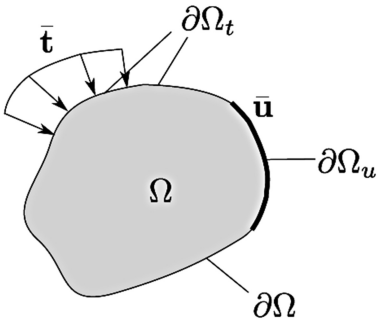

Fig. 2.2 Domain Ω with prescribed displacements $\bar{\mathbf{u}}$ on the Dirichlet boundary $\partial\Omega_u$ and prescribed tractions $\bar{\mathbf{t}}$ on the Neumann boundary $\partial\Omega_t$. Similar boundaries can be defined for the thermal problem, where a given temperature $\bar{T}$ is prescribed on the Dirichlet boundary $\partial\Omega_T$ and a normal heat flux $\bar{q}_n$ is prescribed on the Neumann boundary $\partial\Omega_q$

together with the boundary and initial conditions

$$\mathbf{u} = \bar{\mathbf{u}} \qquad \forall \mathbf{x} \in \partial\Omega_u \tag{2.3}$$

$$\boldsymbol{\sigma} \cdot \mathbf{n} = \bar{\mathbf{t}} \qquad \forall \mathbf{x} \in \partial\Omega_t \tag{2.4}$$

$$T = \bar{T} \qquad \forall \mathbf{x} \in \partial\Omega_T \tag{2.5}$$

$$-\mathbf{q} \cdot \mathbf{n} = \bar{q}_n \qquad \forall \mathbf{x} \in \partial\Omega_q \tag{2.6}$$

$$\mathbf{u}(t=0) = \mathbf{u}_0 \qquad \forall \mathbf{x} \in \Omega \tag{2.7}$$

$$T(t=0) = T_0 \qquad \forall \mathbf{x} \in \Omega \tag{2.8}$$

where the boundary domains fulfill the conditions

$$\partial\Omega = \partial\Omega_u \cup \partial\Omega_t = \partial\Omega_T \cup \partial\Omega_q$$
$$\emptyset = \partial\Omega_u \cap \partial\Omega_t = \partial\Omega_T \cap \partial\Omega_q$$

In preparation of a finite element implementation, Eqs. (2.1) and (2.2) are cast into their weak forms. For that purpose we introduce the function *ansatz* and test spaces

$$\mathbf{V}_u^a = \{\mathbf{v} \in \mathbf{H}^1(\Omega) : \ \mathbf{v} = \bar{\mathbf{u}} \ \forall \mathbf{x} \in \partial\Omega_u\}$$
$$V_T^a = \{v \in H^1(\Omega) : \ v = \bar{T} \ \forall \mathbf{x} \in \partial\Omega_T\}$$
$$\mathbf{V}_u^t = \{\mathbf{v} \in \mathbf{H}^1(\Omega) : \ \mathbf{v} = \mathbf{0} \ \forall \mathbf{x} \in \partial\Omega_u\}$$
$$V_T^t = \{v \in H^1(\Omega) : \ v = 0 \ \forall \mathbf{x} \in \partial\Omega_T\}$$

With $\mathbf{u} \in \mathbf{V}_u^a$, $T \in V_T^a$, $\mathbf{v}_u \in \mathbf{V}_u^t$ and $v_T \in V_T^t$ we find the weak forms

$$\int_\Omega \boldsymbol{\sigma} : \operatorname{grad} \mathbf{v}_u \, \mathrm{d}\Omega = \int_{\partial\Omega_t} \bar{\mathbf{t}} \cdot \mathbf{v}_u \, \mathrm{d}\Gamma + \int_\Omega \mathbf{b} \cdot \mathbf{v}_u \, \mathrm{d}\Omega \tag{2.9}$$

$$\int_\Omega \varrho c_p \frac{\partial T}{\partial t} v_T \, \mathrm{d}\Omega - \int_\Omega \mathbf{q} \cdot \operatorname{grad} v_T \, \mathrm{d}\Omega = \int_{\partial\Omega_q} q_n v_T \, \mathrm{d}\Omega \tag{2.10}$$

As will be outlined in Sect. 2.4, a uni-directional staggered coupling scheme will be used to solve the coupled problem given by Eqs. (2.9) and (2.2). Non-linear constitutive equations for the stresses (cf. Sect. 2.3) motivate an incremental-iterative approach. Based on a known solution at time t, the solution in the next time increment $t + \Delta t$ will be determined iteratively by a Newton–Raphson scheme. For that purpose, a linearisation of Eq. (2.9) is performed around the current state identified by the (global Newton) iteration counter i, leading to the linearized weak form

$$\begin{aligned} &\int_\Omega \operatorname{grad} \mathbf{v}_u : \left. \frac{\mathrm{d}\boldsymbol{\sigma}}{\mathrm{d}\boldsymbol{\epsilon}} \right|_i : \Delta\boldsymbol{\epsilon}^{i+1} \, \mathrm{d}\Omega \\ &\quad = \int_{\partial\Omega_t} \bar{\mathbf{t}}^{t+\Delta t} \cdot \mathbf{v}_u \, \mathrm{d}\Gamma + \int_\Omega \mathbf{b}^{t+\Delta t} \cdot \mathbf{v}_u \, \mathrm{d}\Omega - \int_\Omega \boldsymbol{\sigma}^i : \operatorname{grad} \mathbf{v}_u \, \mathrm{d}\Omega \end{aligned} \tag{2.11}$$

where

$$\mathcal{C} = \frac{\mathrm{d}\boldsymbol{\sigma}}{\mathrm{d}\boldsymbol{\epsilon}} \tag{2.12}$$

is the fourth-order constitutive stiffness tensor.

In the present coupling scheme and for the constitutive assumptions made here, no such step is necessary for Eq. (2.10).

2.2 Finite Element Implementation and the Kelvin Mapping

The Kelvin Mapping of Tensorial Quantities

Commonly, the transition to a standard matrix–vector notation in the context of finite element implementations is performed by replacing three-dimensional symmetric second-order tensors by six-dimensional vectors (using engineering shear strains $\gamma_{ij} = 2\epsilon_{ij}$) and three-dimensional fourth-order tensors by 6×6 matrices. This *Voigt mapping* leads to a different treatment of, e.g., stresses and strains and does not

preserve tensor norms. Here, the *Kelvin mapping* will be preferred which introduces a new 6D basis $\{\mathbf{E}_I\}$ such that the tensor character of all quantities is preserved.

In terms of implementation, OGS-5 is set up using the Voigt mapping with only a few material models integrated with an experimental Kelvin mapping scheme. The integration relies on appropriate transformation routines for both mappings. OGS-6 is entirely designed both in its core and in the implemented constitutive models using the Kelvin mapping.

One possible way of arriving at the Kelvin mapping is to consider the eigenvalue problem of fourth-order tensors in analogy to the more familiar version for second-order tensors. Without going into details, which can be found in Nagel et al. (2016), the super-symmetric fourth-order symmetry projection tensor $\mathcal{I}^{\mathrm{s}}$ with the property $\mathcal{I}^{\mathrm{s}} : \mathbf{A} = \operatorname{sym} \mathbf{A}$ can be written in a Cartesian basis $\{\mathbf{e}_i\}$ and by using $\mathbf{I} = \mathbf{e}_i \otimes \mathbf{e}_i$ as

$$\mathcal{I}^{\mathrm{s}} = \mathbf{I} \underline{\odot} \mathbf{I} = \frac{1}{2} \left[\mathbf{e}_i \otimes \mathbf{e}_j \otimes \mathbf{e}_i \otimes \mathbf{e}_j + \mathbf{e}_i \otimes \mathbf{e}_j \otimes \mathbf{e}_j \otimes \mathbf{e}_i \right] \tag{2.13}$$

and has the six eigentensors (Itskov 2009):

$$\begin{aligned} \mathbf{M}_1 &= \mathbf{e}_1 \otimes \mathbf{e}_1 & \mathbf{M}_4 &= \frac{1}{\sqrt{2}} (\mathbf{e}_1 \otimes \mathbf{e}_2 + \mathbf{e}_2 \otimes \mathbf{e}_1) \\ \mathbf{M}_2 &= \mathbf{e}_2 \otimes \mathbf{e}_2 & \mathbf{M}_5 &= \frac{1}{\sqrt{2}} (\mathbf{e}_2 \otimes \mathbf{e}_3 + \mathbf{e}_3 \otimes \mathbf{e}_2) \\ \mathbf{M}_3 &= \mathbf{e}_3 \otimes \mathbf{e}_3 & \mathbf{M}_6 &= \frac{1}{\sqrt{2}} (\mathbf{e}_1 \otimes \mathbf{e}_3 + \mathbf{e}_3 \otimes \mathbf{e}_1) \end{aligned} \tag{2.14}$$

These eigentensors can be viewed as the basis of the Kelvin mapping. Instead of simply reordering tensor coordinates as done in the Voigt mapping, the Kelvin mapping proceeds from the introduction of a new 6D basis $\{\mathbf{E}_I\}$ based on the original 3D basis $\{\mathbf{e}_i\}$ (compare Mehrabadi and Cowin 1990) by setting

$$\mathbf{E}_I = \mathbf{M}_I (\mathcal{I}^{\mathrm{s}}) \; \forall I = 1, \ldots, 6 \tag{2.15}$$

In other words, this basis is identical to the eigentensors of the symmetry projection tensor $\mathcal{I}^{\mathrm{s}}$, compare Eq. (2.14).

Thus, exemplary tensors with the necessary symmetries can equivalently be written in the various bases

$$\mathbf{A} = A_{ij} \mathbf{e}_i \otimes \mathbf{e}_j = A_I \mathbf{E}_I \quad \text{with} \quad A_I = \mathbf{A} : \mathbf{E}_I \tag{2.16}$$

$$\boldsymbol{\mathcal{A}} = A_{ijkl} \mathbf{e}_i \otimes \mathbf{e}_j \otimes \mathbf{e}_k \otimes \mathbf{e}_l = A_{IJ} \mathbf{E}_I \otimes \mathbf{E}_J \quad \text{with} \quad A_{IJ} = \mathbf{E}_I : \boldsymbol{\mathcal{A}} : \mathbf{E}_J \tag{2.17}$$

At this stage, we introduce the following short-hand for the vector of tensor coordinates A_I of a second-order tensor in the Kelvin basis: $\underline{A}$. Similarly, the matrix of tensor coordinates A_{IJ} of a fourth-order tensor in the Kelvin basis will be abbreviated by $\mathbb{A}$.

One can see that, similar to the Voigt mapping, the coordinates of second- and fourth-order tensors can now be represented as six-dimensional vectors and matrices. However, the tensor character of all quantities is still preserved. Note further that the coordinates of the Kelvin-mapping of a fourth-order tensor $\mathbf{A} \otimes \mathbf{A}$ simply follow from the coordinate matrix of the dyadic product of the Kelvin mapped vectors. Thus, the same notation can be employed in both cases.

For numerical implementation, the coordinates of the Kelvin-mapped stress and strain tensors can now be used in a vector format

$$\sigma_{ij} \rightarrow \underline{\sigma} = \left[\sigma_{11}\ \sigma_{22}\ \sigma_{33}\ \sqrt{2}\sigma_{12}\ \sqrt{2}\sigma_{23}\ \sqrt{2}\sigma_{13}\ \right]^{\mathrm{T}} \tag{2.18}$$

$$\epsilon_{ij} \rightarrow \underline{\epsilon} = \left[\epsilon_{11}\ \epsilon_{22}\ \epsilon_{33}\ \sqrt{2}\epsilon_{12}\ \sqrt{2}\epsilon_{23}\ \sqrt{2}\epsilon_{13}\ \right]^{\mathrm{T}} \tag{2.19}$$

which have the same structure regardless of whether they are stresses or strains. This has the important consequence that tensor norms are preserved when using the Kelvin mapping. This further simplifies the implementation of constitutive models as it makes any distinction of stress- or strain-type quantities entering mathematical operations obsolete (Nagel et al. 2016).

Finite Element Implementation

The domain of interest is split into standard finite elements characterised by a set of nodal shape functions $N^a(\mathbf{x})$. The sought solution vector $\underline{u}$ (for a more uniform notation we write $\underline{u}$ even though no Kelvin mapping is performed on the original vector $\mathbf{u}$) in a point is approximated by

$$\underline{u} \approx \underline{\tilde{u}} = \sum_{a}^{n_{\mathrm{n}}} N^a \underline{\hat{u}}_a = \mathbb{N}\underline{\hat{u}} \tag{2.20}$$

where

$$\underline{\hat{u}} = \left[\hat{u}_1^1 \cdots \hat{u}_1^{n_{\mathrm{n}}}\ \hat{u}_2^1 \cdots \hat{u}_2^{n_{\mathrm{n}}}\ \hat{u}_3^1 \cdots \hat{u}_3^{n_{\mathrm{n}}}\right]^{\mathrm{T}} \tag{2.21}$$

is the nodal displacement vector of the element containing the point at which $\underline{u}$ is evaluated, $\mathbb{N}$ is the element matrix of shape functions and n_{n} is the number of nodes of said element. In the isoparametric concept employed here, the position vector $\underline{x}$ and the test function $\underline{v}$ are approximated likewise. Similarly, the $\mathbb{B}$-matrix containing the gradients of the shape functions can be introduced to enable the calculation of strain vectors from the nodal displacements (for details see, e.g., Zienkiewicz et al. 2005–2006):

$$\underline{\epsilon} = \operatorname{sym}\operatorname{grad}\underline{u} = \mathbb{B}\underline{\hat{u}} \quad \text{and} \quad \operatorname{sym}\operatorname{grad}\underline{v} = \mathbb{B}\underline{\hat{v}} \tag{2.22}$$

with the slightly modified $\mathbb{B}$-matrix

$$\mathbb{B}_0 = \begin{pmatrix} N^1_{,1} \ \dots \ N^{n_\mathrm{n}}_{,1} & 0 \cdots 0 & 0 \cdots 0 \\ 0 \cdots 0 & N^1_{,2} \dots \ N^{n_\mathrm{n}}_{,2} & 0 \cdots 0 \\ 0 \cdots 0 & 0 \cdots 0 & N^1_{,3} \ \dots \ N^{n_\mathrm{n}}_{,3} \\ \left[N^1_{,2} \ \dots \ N^{n_\mathrm{n}}_{,2}\right]/\sqrt{2} & \left[N^1_{,1} \ \dots \ N^{n_\mathrm{n}}_{,1}\right]/\sqrt{2} & 0 \cdots 0 \\ 0 \cdots 0 & \left[N^1_{,3} \ \dots \ N^{n_\mathrm{n}}_{,3}\right]/\sqrt{2} & \left[N^1_{,2} \ \dots \ N^{n_\mathrm{n}}_{,2}\right]/\sqrt{2} \\ \left[N^1_{,3} \ \dots \ N^{n_\mathrm{n}}_{,3}\right]/\sqrt{2} & 0 \cdots 0 & \left[N^1_{,1} \ \dots \ N^{n_\mathrm{n}}_{,1}\right]/\sqrt{2} \end{pmatrix} \tag{2.23}$$

Substitution of these relations into Eq. (2.11) allows the elimination of the arbitrary nodal values $\underline{\hat{v}}$ of the test functions and produces the equation system for each elemental domain Ω^e:

$$\int_{\Omega^e} \mathbb{B}^\mathrm{T} \mathbb{C}^i \mathbb{B} \, \mathrm{d}\Omega \ \Delta \underline{\hat{u}}^{i+1} = \int_{\partial\Omega^e_t} \mathbb{N}^\mathrm{T} \underline{\bar{t}}^{t+\Delta t} \, \mathrm{d}\Gamma + \int_{\Omega^e} \mathbb{N}^\mathrm{T} \varrho \underline{b}^{t+\Delta t} \, \mathrm{d}\Omega - \int_{\Omega^e} \mathbb{B}^\mathrm{T} \underline{\sigma}^i \, \mathrm{d}\Omega \tag{2.24}$$

The integral on the left-hand side defines the stiffness matrix $\mathbb{K}$, the right-hand side defines the residual vector $\underline{\psi}$ such that the linearised system reads

$$\mathbb{K}^i \Delta \underline{\hat{u}}^{i+1} = \underline{\psi}^i \tag{2.25}$$

The contributions of all elements are assembled into the global problem which is then solved for the vector of unknown displacement increments $\Delta \underline{\hat{u}}^{i+1}$.

In summary, a constitutive equation for the stresses is required to correctly calculate the residual vector $\underline{\psi}^i$ on the right-hand side of Eq. (2.24) as well as the usually solution dependent $\mathbb{C}^i$-matrix containing the material moduli in an algorithmically consistent manner (Simo and Hughes 1998).

For similar finite element schemes in a finite-strain setting, see, e.g., Görke et al. (2010, 2012a), Zienkiewicz et al. (2005–2006), and Bathe (2014). For an extension of the Kelvin mapping to the finite-strain context, refer to Nagel et al. (2016).

2.3 Integration of Inelastic Constitutive Models

General Aspects

In order to determine the stresses $\boldsymbol{\sigma}^i$ and the stiffness tensor $\boldsymbol{\mathcal{C}}^i$ or, more accurately, their coordinate matrices in Kelvin mapping $\underline{\sigma}^i$ and $\mathbb{C}^i$ from Eq. (2.24), constitutive relations are required.

In the linear elastic case, stress follows directly—independent of loading path and rate—from strain and the stiffness matrix has constant entries, rendering Eq. (2.24)

linear. The tensorial relations for linear elasticity (using the Lamé constants)

$$\boldsymbol{\sigma} = \lambda\,(\boldsymbol{\epsilon} : \mathbf{I})\mathbf{I} + 2\mu\boldsymbol{\epsilon} \tag{2.26}$$

$$\boldsymbol{\mathcal{C}} = \lambda\mathbf{I} \otimes \mathbf{I} + 2\mu\mathbf{I} \odot \mathbf{I} \tag{2.27}$$

hold independent of the particular tensor basis (i.e., also for the Kelvin mapping) and translate into the following Kelvin-mapped tensor coordinate matrices:

$$\underline{\sigma} = \begin{pmatrix} 2\mu\epsilon_{11} + \lambda\mathrm{tr}\,\boldsymbol{\epsilon} \\ 2\mu\epsilon_{22} + \lambda\mathrm{tr}\,\boldsymbol{\epsilon} \\ 2\mu\epsilon_{33} + \lambda\mathrm{tr}\,\boldsymbol{\epsilon} \\ 2\mu\sqrt{2}\epsilon_{12} \\ 2\mu\sqrt{2}\epsilon_{23} \\ 2\mu\sqrt{2}\epsilon_{13} \end{pmatrix} = \lambda(\underline{\epsilon} \cdot \underline{I})\underline{I} + 2\mu\underline{\epsilon} \tag{2.28}$$

$$\mathbb{C} = \begin{pmatrix} 2\mu+\lambda & \lambda & \lambda & 0 & 0 & 0 \\ \lambda & 2\mu+\lambda & \lambda & 0 & 0 & 0 \\ \lambda & \lambda & 2\mu+\lambda & 0 & 0 & 0 \\ 0 & 0 & 0 & 2\mu & 0 & 0 \\ 0 & 0 & 0 & 0 & 2\mu & 0 \\ 0 & 0 & 0 & 0 & 0 & 2\mu \end{pmatrix} \tag{2.29}$$

Considering general inelastic material models, these constitutive relationships follow from a set of differential and algebraic equations (DAEs) of varying non-linearity. In other words, stresses don't follow in an explicit manner from total strains and the stiffness matrix is no longer constant.

Integration Algorithm

In order to efficiently solve the non-linearities a local Newton–Raphson procedure is introduced consistent with its global equivalent. *Local* in this context refers to performing the stress integration in each integration point of the quadrature rule employed to numerically approximate the integrals in Eq. (2.24) by sums. *Global* refers to the entire equation system (2.25) assembled over all finite elements of the domain. More details on the following can be found in Nagel et al. (2017) and the references therein.

The differential-algebraic equation system necessary for the integration of the stress increments is compactly written as

$$\underline{0} = \underline{r}(\underline{z}, \underline{\epsilon}^i) \tag{2.30}$$

where $\underline{r}$ represents the residual vector describing the evolution equations for stresses and internal variables, as well as constraints (e.g., the consistency condition in elasto-plasticity). Note that in the local iterations to solve the above equation system, $\underline{\epsilon}^i$ from the global iteration is considered fixed. The state vector $\underline{z}$ contains the stress vector as well as the constitutive model's internal state variables ($\underline{\kappa}_k$, κ_k):

$$\underline{z} = (\underline{\sigma}^{\mathrm{T}}, \underline{\kappa}_k^{\mathrm{T}}, \kappa_k)^{\mathrm{T}} \tag{2.31}$$

The evolution equations most often involve rates in the form of first order time derivatives. Considering the general ordinary differential equation

$$\dot{y} = f(y) \,, \tag{2.32}$$

time discretisation of the rate quantities in the functionals is based here on a generalised single step scheme. We write for a time step in the interval $[t, t + \Delta t]$

$$y^{t+\Delta t} = y^t + \Delta t \left[\alpha\, f^{t+\Delta t} + (1-\alpha)\, f^t\right] \tag{2.33}$$

which includes the schemes

$$\alpha = \begin{cases} 0 & \text{Euler forward (explicit)} \\ 0.5 & \text{Crank–Nicolson} \\ 1 & \text{Euler backward (implicit)} \end{cases} \tag{2.34}$$

With this relationship, a rate of change at time $t + \Delta t$ can be approximated based solely on known quantities and the unknown primary variable at time $t + \Delta t$:

$$\dot{y}^{t+\Delta t} = \frac{y^{t+\Delta t}}{\alpha \Delta t} - \frac{y^t}{\alpha \Delta t} - \frac{1-\alpha}{\alpha} f^t \tag{2.35}$$

Note that for $\alpha = 0$, the above relationship cannot be used directly but the rate at time t is used directly and exclusively. A Taylor series expansion of the differential-algebraic system yields the iteration procedure for the local stress integration

$$-\underline{r}^j = \left.\frac{\partial \underline{r}}{\partial \underline{z}}\right|_j \Delta \underline{z}^{j+1} \tag{2.36}$$

It shall be mentioned here that the resulting solution update can be dampened by a factor α_{LS} determined from a line-search procedure

$$\underline{z}^{j+1} = \underline{z}^j + \alpha_{\mathrm{LS}} \Delta \underline{z}^{j+1} \tag{2.37}$$

where $\alpha_{\mathrm{LS}} \in (0, 1]$ would be the most common but not the only choice. Line-search algorithms are motivated by either the acceleration of convergence or the achievement of convergence itself in regions where the standard Newton–Raphson

algorithm would diverge. Numerous methods are available to determine the value of α_{LS} (Jeremic 2001; Seifert and Schmidt 2008; Zienkiewicz et al. 2005–2006).

Once the iteration has converged, we find the consistent tangent matrix for the global iteration using the total differential of $\underline{r}$ and the fact that the first entry in $\underline{z}$ is always $\underline{\sigma}$:

$$\frac{\mathrm{d}\underline{r}}{\mathrm{d}\underline{\epsilon}^{t+\Delta t}} = \frac{\partial \underline{r}}{\partial \underline{\epsilon}^{t+\Delta t}} + \left(\left. \frac{\partial \underline{r}}{\partial \underline{z}} \right|_{t+\Delta t} \right) \frac{\mathrm{d}\underline{z}}{\mathrm{d}\underline{\epsilon}^{t+\Delta t}} = \underline{0} \tag{2.38}$$

The first entry of the solution $\mathrm{d}\underline{z}/\mathrm{d}\underline{\epsilon}^{t+\Delta t}$ to the resulting linear system

$$\left(\left. \frac{\partial \underline{r}}{\partial \underline{z}} \right|_{t+\Delta t} \right) \frac{\mathrm{d}\underline{z}}{\mathrm{d}\underline{\epsilon}^{t+\Delta t}} = -\frac{\partial \underline{r}}{\partial \underline{\epsilon}^{t+\Delta t}} \tag{2.39}$$

is the sought tangent matrix $\mathbb{C}^i$. Thus, the tangent modulus matrix can be computed with very little extra effort based on the already known Jacobian from the local stress-update procedure and is automatically consistent with the integration algorithm chosen. The latter point is of importance for achieving the best possible convergence of the global problem (Simo and Hughes 1998; Zienkiewicz et al. 2005–2006).

2.4 Thermo-Mechanical Coupling in OGS

When considering applications such as nuclear waste storage, CAES, etc., thermal fields influence the material behaviour of the rock salt by lowering elastic moduli and viscosity parameters or by increasing healing rates, as outlined in Nagel et al. (2017). For a general thermo-mechanical coupling, a monolithic scheme is conceivable where the coupling matrices result from the dependence of one PDE on the primary variable of the other:

$$\begin{pmatrix} \mathbb{K}_{uu} & \mathbb{K}_{uT} \\ \mathbb{K}_{Tu} & \mathbb{K}_{TT} \end{pmatrix} \begin{pmatrix} \Delta \underline{u} \\ \Delta \underline{T} \end{pmatrix} = \begin{pmatrix} \underline{\psi}_u \\ \underline{\psi}_T \end{pmatrix} \tag{2.40}$$

A monolithic THM scheme is used, for example, to simulate freezing processes in OGS-6. In general, mechanical work can be partially dissipated into heat and thus lead to local temperature changes. However, for the strain rates and boundary conditions relevant here, the coupling to temperature fields can be described as uni-directional, i.e. the temperature distribution affects the mechanical problem but not the other way around. Therefore, an efficient solution technique is to couple the thermal and mechanical initial boundary value problems (IBVP) in a

staggered/partitioned fashion. In other words, with ϱc_p the volumetric isobaric heat capacity and $\boldsymbol{\lambda}$ the thermal conductivity tensor, the PDE-system

$$\text{PDE 1:} \quad 0 = \varrho c_p \frac{\partial T}{\partial t} - \operatorname{div}\left(\boldsymbol{\lambda} \operatorname{grad} T\right) \tag{2.41}$$

$$\text{PDE 2:} \quad 0 = \operatorname{div} \boldsymbol{\sigma}\left(\mathbf{u}, T\right) + \varrho \mathbf{b} = \mathbf{0} \tag{2.42}$$

is addressed by an algorithm which solves the PDE governing one of the primary variables (temperature and displacement) while keeping the other fixed and iterating until convergence. Choosing an FE residual formulation this may be illustrated by

$$\mathbb{K}_{TT} \Delta \underline{T} = \underline{\psi}_T - \underline{f}(\underline{u}) \text{ at fixed } \underline{u} \quad \leftrightarrow \quad \mathbb{K}_{uu} \Delta \underline{u} = \underline{\psi}_u - \underline{f}(\underline{T}) \quad \text{ at fixed } \underline{T}$$

where the residuals may be modified by source term-like contributions from the other coupled processes. In case of the one way coupling considered here, i.e. $\mathbb{K}_{Tu} = \mathbb{O}$, the thermal IBVP is solved first, followed by the solution of the mechanical IBVP without any further iteration between both processes necessary. Details on weak forms of coupled problems and possible implementations can be found in standard references, e.g. Lewis and Schrefler (1998). For a detailed overview on coupling strategies in numerical simulations, we refer the reader to Markert (2013).

The inclusion of temperature-dependent material parameters and thermal strains will be an inherent part of the material models and algorithms used below.

2.5 Constitutive Models

Thermal Process

In addition to $\dot{h} = c_p \dot{T}$, only one other constitutive relation is required to close Eq. (2.2) by connecting the temperature field with the heat flux vector. It is here taken simply as the linear Fourier's law:

$$\mathbf{q} = -\boldsymbol{\lambda} \operatorname{grad} T \tag{2.43}$$

Mechanical Process

Linear elasticity is insufficient to describe the deformation behaviour of rock salt under most practically relevant loading conditions. Viscoelastic and viscoplastic material models represent the more appropriate choice. Various material models are available in OGS for that purpose (Kolditz et al. 2012, 2014, 2016; Nagel et al. 2017), e.g. Norton and various BGR creep laws (Hunsche and Schulze 1994), the

LUBBY2 (Heusermann et al. 1983, 2003) and a variant of the Minkley material model (Minkley and Mühlbauer 2007; Minkley et al. 2001). These models follow different concepts in calculating the creep strain rate as well as its temperature dependence:

Norton $$\dot{\boldsymbol{\epsilon}}_{\mathrm{cr}} = A \left(\frac{\sigma_{\mathrm{eff}}}{\sigma_0} \right)^n \frac{\boldsymbol{\sigma}^{\mathrm{D}}}{\sigma_{\mathrm{eff}}}$$

BGRa $$\dot{\boldsymbol{\epsilon}}_{\mathrm{cr}} = \frac{3}{2} A \left(\frac{\sigma_{\mathrm{eff}}}{\sigma_0} \right)^n \exp\left(-\frac{Q}{RT} \right) \frac{\boldsymbol{\sigma}^{\mathrm{D}}}{\sigma_{\mathrm{eff}}}$$

BGRb $$\dot{\boldsymbol{\epsilon}}_{\mathrm{cr}} = \frac{3}{2} \left[A_1 \left(\frac{\sigma_{\mathrm{eff}}}{\sigma_0} \right)^{n_1} \exp\left(-\frac{Q_1}{RT} \right) + A_2 \left(\frac{\sigma_{\mathrm{eff}}}{\sigma_0} \right)^{n_2} \exp\left(-\frac{Q_2}{RT} \right) \right] \frac{\boldsymbol{\sigma}^{\mathrm{D}}}{\sigma_{\mathrm{eff}}}$$

LUBBY2 See Eqs. (2.44)–(2.51)

Minkley See Eqs. (2.52)–(2.61)

Here, we focus on the latter two which both capture stress- and temperature-dependent transient and stationary creep phases as indicated by their rheological analogues depicted in Fig. 2.3. Additionally, the Minkley model can describe plastic effects which include strain hardening and softening as well as dilatancy (Minkley and Mühlbauer 2007; Minkley et al. 2001).

LUBBY2

The following set of equations describes the temperature-dependent LUBBY2 model (compare Fig. 2.3a):

$$\boldsymbol{\sigma} = K_{\mathrm{M}}(e - 3\alpha_T \Delta T)\mathbf{I} + 2G_{\mathrm{M}} \left[\boldsymbol{\epsilon}^{\mathrm{D}} - \boldsymbol{\epsilon}_{\mathrm{M}}^{\mathrm{D}} - \boldsymbol{\epsilon}_{\mathrm{K}}^{\mathrm{D}} \right] \tag{2.44}$$

$$\dot{\boldsymbol{\epsilon}}_{\mathrm{K}}^{\mathrm{D}} = \frac{1}{2\eta_{\mathrm{K}}} (\boldsymbol{\sigma}^{\mathrm{D}} - 2G_{\mathrm{K}} \boldsymbol{\epsilon}_{\mathrm{K}}^{\mathrm{D}}) \tag{2.45}$$

$$\dot{\boldsymbol{\epsilon}}_{\mathrm{M}}^{\mathrm{D}} = \frac{1}{2\eta_{\mathrm{M}}} \boldsymbol{\sigma}^{\mathrm{D}} \tag{2.46}$$

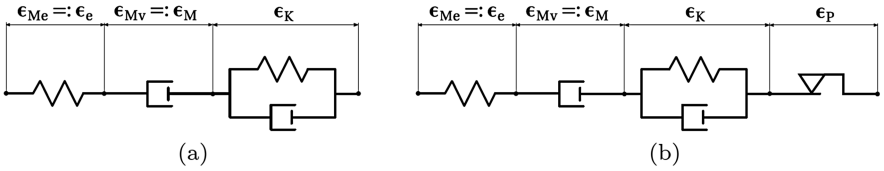

Fig. 2.3 Rheological models of the (**a**) LUBBY2 and the (**b**) Minkley material models

where the viscosities and (visco)elastic moduli are functions of both stress and strain (Böttcher et al. 2017; Du et al. 2012)

$$\eta_{\mathrm{M}} = \eta_{\mathrm{M0}} \exp(m_1 \sigma_{\mathrm{eff}}/\sigma_0) \exp[Q(T_{\mathrm{ref}} - T)/(RTT_{\mathrm{ref}})] \tag{2.47}$$

$$\eta_{\mathrm{K}} = \eta_{\mathrm{K0}} \exp(m_2 \sigma_{\mathrm{eff}}/\sigma_0) \tag{2.48}$$

$$G_{\mathrm{K}} = G_{\mathrm{K0}} \exp(m_{\mathrm{G}} \sigma_{\mathrm{eff}}/\sigma_0) \tag{2.49}$$

$$K_{\mathrm{M}} = K_{\mathrm{M0}} + m_{\mathrm{KT}}(T - T_{\mathrm{ref}}) \tag{2.50}$$

$$G_{\mathrm{M}} = G_{\mathrm{M0}} + m_{\mathrm{GT}}(T - T_{\mathrm{ref}}) \tag{2.51}$$

$$\text{with } \sigma_{\mathrm{eff}} = \sqrt{\frac{3}{2}\boldsymbol{\sigma}^{\mathrm{D}} : \boldsymbol{\sigma}^{\mathrm{D}}}$$

For more details on the implementation, see Nagel et al. (2017).

Minkley

The Minkley model as implemented in OGS and indicated in Fig. 2.3b is described by the following set of equations:

$$\boldsymbol{\sigma} = K_{\mathrm{M}}(e - e_{\mathrm{P}} - 3\alpha_T \Delta T)\mathbf{I} + 2G_{\mathrm{M}}\left(\boldsymbol{\epsilon}^{\mathrm{D}} - \boldsymbol{\epsilon}_{\mathrm{P}}^{\mathrm{D}} - \boldsymbol{\epsilon}_{\mathrm{K}}^{\mathrm{D}} - \boldsymbol{\epsilon}_{\mathrm{M}}^{\mathrm{D}}\right) \tag{2.52}$$

$$\dot{\boldsymbol{\epsilon}}_{\mathrm{K}}^{\mathrm{D}} = \frac{1}{2\eta_{\mathrm{K}}}(\boldsymbol{\sigma}^{\mathrm{D}} - 2G_{\mathrm{K}}\boldsymbol{\epsilon}_{\mathrm{K}}^{\mathrm{D}}) \tag{2.53}$$

$$\dot{\boldsymbol{\epsilon}}_{\mathrm{M}}^{\mathrm{D}} = \frac{1}{2\eta_{\mathrm{M}}}\boldsymbol{\sigma}^{\mathrm{D}} \tag{2.54}$$

$$\dot{\boldsymbol{\epsilon}}_{\mathrm{P}}^{\mathrm{D}} = \lambda \frac{\partial G_{\mathrm{F}}}{\partial \boldsymbol{\sigma}} : \boldsymbol{\mathcal{P}}^{\mathrm{D}} \tag{2.55}$$

$$\dot{e}_{\mathrm{P}} = \lambda \frac{\partial G_{\mathrm{F}}}{\partial \boldsymbol{\sigma}} : \boldsymbol{\mathcal{P}}^{\mathrm{S}} : \mathbf{I} \tag{2.56}$$

$$\dot{\epsilon}_{\mathrm{P\,eff}} = \sqrt{\frac{2}{3}\dot{\boldsymbol{\epsilon}}_{\mathrm{p}}^{\mathrm{D}} : \dot{\boldsymbol{\epsilon}}_{\mathrm{p}}^{\mathrm{D}}} \tag{2.57}$$

$$F = 0 \tag{2.58}$$

Again, the model is characterised by stress and temperature dependencies of viscosities and elastic moduli:

$$\eta_{\mathrm{M}} = \frac{\eta_{\mathrm{M0}} \exp[Q(T_{\mathrm{ref}} - T)/(RTT_{\mathrm{ref}})]}{\sinh\left[m\left(\frac{\sigma_{\mathrm{eff}}}{\sigma_0}\right)^n\right]} \tag{2.59}$$

$$K_{\mathrm{M}} = K_{\mathrm{M0}} + m_{\mathrm{KT}}(T - T_{\mathrm{ref}}) \tag{2.60}$$

$$G_{\mathrm{M}} = G_{\mathrm{M0}} + m_{\mathrm{GT}}(T - T_{\mathrm{ref}}) \tag{2.61}$$

The yield function in Eq. (2.58) and the plastic potential required for Eqs. (2.55) and (2.56) were taken as Mohr–Coulomb types with corner smoothing:

$$F = \begin{cases} \dfrac{I_1}{3}\sin\phi + \sqrt{J_2}\left(\cos\theta - \dfrac{1}{\sqrt{3}}\sin\phi\sin\theta\right) - c\cos\phi & |\theta| < \theta_{\mathrm{T}} \\ \dfrac{I_1}{3}\sin\phi + \sqrt{J_2}\,(A - B\sin 3\theta) - c\cos\phi & |\theta| \geq \theta_{\mathrm{T}} \end{cases} \tag{2.62}$$

where c and ϕ are the cohesion and friction angle, respectively, and

$$A = \frac{1}{3}\cos\theta_{\mathrm{T}}\left[3 + \tan\theta_{\mathrm{T}}\tan 3\theta_{\mathrm{T}} + \frac{1}{\sqrt{3}}\mathrm{sign}\,\theta(\tan 3\theta_{\mathrm{T}} - 3\tan\theta_{\mathrm{T}})\sin\phi\right] \tag{2.63}$$

$$B = \frac{1}{3}\frac{1}{\cos 3\theta_{\mathrm{T}}}\left[\mathrm{sign}\,\theta\sin\theta_{\mathrm{T}} + \frac{1}{\sqrt{3}}\sin\phi\cos\theta_{\mathrm{T}}\right] \tag{2.64}$$

The plastic potential differs from the yield surface in order to more accurately estimate dilatancy, but has an analogous structure:

$$G_{\mathrm{F}} = \begin{cases} \dfrac{I_1}{3}\sin\psi + \sqrt{J_2}\left(\cos\theta - \dfrac{1}{\sqrt{3}}\sin\psi\sin\theta\right) & |\theta| < \theta_{\mathrm{T}} \\ \dfrac{I_1}{3}\sin\psi + \sqrt{J_2}\left(A' - B'\sin 3\theta\right) & |\theta| \geq \theta_{\mathrm{T}} \end{cases} \tag{2.65}$$

where ψ is the dilatancy angle. A' and B' follow from Eqs. (2.63), (2.64) by substituting the friction angle with the dilatancy angle. Hardening or softening is here by a smoothly differentiable law which captures hardening, followed by softening up to a defined residual cohesion (compare also Fig. 3.8):

$$c = c_{\mathrm{res}} + (c_0 - c_{\mathrm{res}})\left(1 + A_1\sin\frac{\epsilon_{\mathrm{P\,eff}}}{A_2}\right)\left(1 - \frac{1}{1 + \exp\left[-B_1(\epsilon_{\mathrm{P\,eff}} - B_2)\right]}\right) \tag{2.66}$$

For more details on the implementation, see Nagel et al. (2017). The implementation of the LUBBY2 and Minkley models is verified against analytical solutions in Kolditz et al. (2014, 2016) and Nagel et al. (2017).

Furthermore, a simple viscoplastic regularisation of the Perzyna type can be employed (de Borst and Heeres 2002; Heeres et al. 2002; Wang et al. 1997): we allow stress states with $F > 0$ by introducing a regularisation viscosity η_{reg} and set

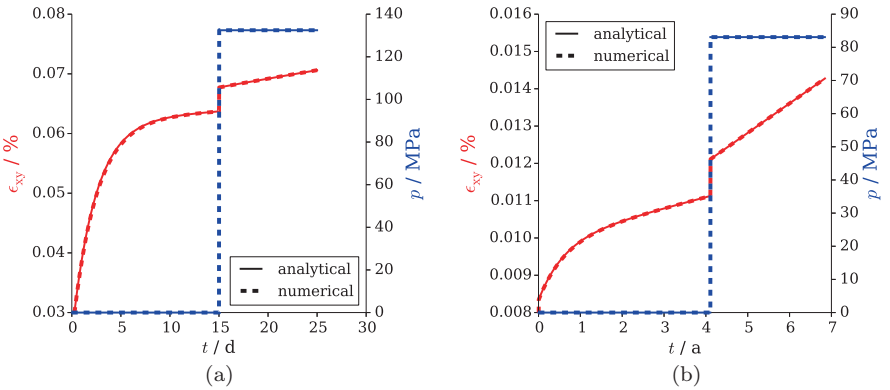

Fig. 2.4 Results of a simulated simple shear creep test for the (**a**) LUBBY2 model and the (**b**) Minkley model. About half-way through the test, a temperature jump was imposed causing an immediate change in the elastic response visible as a jump in the shear strain curve (*red*), a significant hydrostatic pressure (*blue*) due to isochoric confinement of the sample, as well as an increased creep rate. Details and parameters used can be found in Nagel et al. (2017)

$$\dot{\boldsymbol{\epsilon}}_{\mathrm{P}} = \frac{\langle \zeta(F) \rangle}{\eta_{\mathrm{reg}}} \frac{\partial G_{\mathrm{F}}}{\partial \boldsymbol{\sigma}} \tag{2.67}$$

A typical formulation for $\zeta(F)$ is

$$\zeta(F) = \left(\frac{F}{C} \right)^n \tag{2.68}$$

where—to normalise F—a common choice for C is the initial yield stress. For the sake of simplicity, $n = 1$ and $C = G_{\mathrm{M}}$ were chosen here so that the consistency condition in Eq. (2.58) is replaced by

$$\lambda \eta_{\mathrm{reg}} = \langle \zeta(F) \rangle = \frac{\langle F \rangle}{G_{\mathrm{M}}} \tag{2.69}$$

Note that a rate-independent formulation is recovered for $\eta_{\mathrm{reg}} = 0$.

Viscoplastic regularisation works by a load-transfer mechanism: if deformation starts to localise in a finite band of element-width, the increase of the deformation rate in that band in conjunction with the viscous law causes a stiffening of the band and thus a preferential deformation of adjacent element layers (Niazi et al. 2013). This mechanism prevents excessive localisation. Mathematically, this rate-dependence yields a positive-definite tangent operator and hence a well-posed, regularised problem (Forest et al. 2004).

Coupling

In addition to the process coupling (compare also Sect. 2.4) via the effect of thermal expansion[2] included in Eqs. (2.44) and (2.52), the temperature field influences the material behaviour by altering the elastic and creep properties through a temperature-dependent parameterisation of the constitutive models, cf. Eqs. (2.47)–(2.51) and (2.59)–(2.61).

In a stress-controlled simple shear test, for which an analytical solution can easily be found, all effects can be illustrated, as shown in Fig. 2.4 for both the Minkley and the LUBBY2 material models.

[2]Other such coupling effects like heat of dissipation, thermoelastic or entropic effects are neglected here.

http://www.springer.com/978-3-319-56960-4

Computational Geotechnics
Storage of Energy Carriers
Nagel, Th.; Böttcher, N.; Görke, U.-J.; Kolditz, O.
2017, XII, 70 p. 29 illus., 26 illus. in color., Softcover
ISBN: 978-3-319-56960-4